

# Microstructuring of carbon/tin quantum dots via a novel photolithography and pyrolysis-reduction process

Xufeng Hong<sup>1</sup>, Liang He<sup>1,2</sup> (✉), Xinyu Ma<sup>1</sup>, Wei Yang<sup>1</sup>, Yiming Chen<sup>1</sup>, Lei Zhang<sup>1</sup>, Haowu Yan<sup>1</sup>, Zhaohuai Li<sup>1</sup>, and Liqiang Mai<sup>1,3</sup> (✉)

<sup>1</sup> State Key Laboratory of Advanced Technology for Materials Synthesis and Processing, Wuhan University of Technology, Wuhan 430070, China

<sup>2</sup> Department of Materials Science and NanoEngineering, Rice University, Houston, TX 77005, USA

<sup>3</sup> Department of Chemistry, University of California, Berkeley, CA 94720, USA

Received: 22 January 2017

Revised: 6 March 2017

Accepted: 12 March 2017

© Tsinghua University Press and Springer-Verlag Berlin Heidelberg 2017

## KEYWORDS

carbon,  
micro-supercapacitors,  
quantum dots,  
photolithography,  
microdevices

## ABSTRACT

A novel microfabrication process based on optimized photolithography combined with pyrolysis-reduction is proposed to fabricate interdigital porous carbon/tin quantum dots (C/Sn QDs) microelectrodes. C/Sn QDs active microelectrodes are also employed as current collectors of a micro-supercapacitor (MSC). A uniform dispersion of Sn QDs (diameter of ~3 nm) in the carbon matrix is achieved using our facile and controllable microfabrication process. The as-fabricated C/Sn QDs MSC obtained by carbonization at 900 °C exhibits a higher areal specific capacitance (5.79 mF·cm<sup>-2</sup>) than that of the pyrolyzed carbon-based MSC (1.67 mF·cm<sup>-2</sup>) and desirable cycling stability (93.3% capacitance retention after 5,000 cyclic voltammetry cycles). This novel microfabrication process is fully compatible with micromachining technologies, showing great potential for large-scale fine micropatterning of carbon-based composites for applications in micro/nano devices.

## 1 Introduction

As electric power is widely employed in various systems, the development of highly efficient energy storage systems is becoming a critical issue [1]. Supercapacitors (SCs) have drawn a great attention being an essential energy storage device, exhibiting a high power density, high cycling stability, and rapid charging–discharging ability as compared with traditional batteries [2–4]. SCs exhibit advantages to

partly replace traditional batteries in some applications, and substantial efforts have been made to obtain high-performance SCs by optimizing of their structure, electrode materials, and fabrication technologies [5–7]. Furthermore, due to their high tolerance for instant large electric current and energy discharge, SCs are useful in pulse and transient high power electric supply [2]. A micro-supercapacitor (MSC) is a kind of SCs that is used as an energy storage component in microdevices/systems and is highly important

Address correspondence to Liang He, hel@whut.edu.cn; Liqiang Mai, mlq518@whut.edu.cn

in modern portable electronic products [6, 8]. As a charging storage component at the electrode–electrolyte interface, MSC can achieve areal capacitance of 5–20  $\mu\text{F}\cdot\text{cm}^{-2}$  [3]. The specific areal capacitance of MSCs is highly dependent on the active electrode materials. Carbonaceous materials, such as pyrolyzed carbon, carbon fibers, carbon nanotubes and graphene are the commonly used electrode materials in MSCs [3, 9]. Among carbonaceous materials, pyrolyzed carbon-based microelectrodes show a great potential for applications in MSCs since the carbon micro-electromechanical system (C-MEMS) enables their fully controllable and compatible integration into microdevices/systems [10–12]. In addition, pyrolyzed carbon exhibits unique advantages, such as chemical inertness, high thermal stability, relatively high specific surface area (SSA), high electrical conductivity and abundance, which attracts growing attention [13–16].

Chen et al. fabricated an ultra-thin, flexible MSC based on photolithography technique, which is highly compatible to enable co-integration with other electronic components [17]. Besides, C-MEMS is a unique platform based on micro/nano technologies including design, microfabrication and construction of various carbon micro/nano structures [12]. The high-yield microfabrication processes proposed for C-MEMS have been applied to the microstructuring of photoresist-derived carbon, which exhibits outstanding advantages, such as the precise control of the microstructures and high repeatability [18]. Photoresist-derived carbon has been investigated for applications in high-performance microdevices/systems, such as 3-dimensional (3D) microbatteries and on-chip MSCs [18–26]. Moreover, various geometries of carbon microelectrodes, even complicated 3D pyrolyzed carbon microelectrodes, can be fabricated by photolithography and a subsequent pyrolysis process, demonstrating their wide applications in MSCs [10, 11, 27–29].

High-performance MSCs based on pyrolyzed carbon microelectrodes have been investigated and optimized [19, 30]. The performance of pyrolyzed carbon mainly depends on the precursor, carbonization temperature and atmosphere. However, there are some limitations in enhancing its performance by optimizing these parameters. Therefore, the formation of composites of pyrolyzed carbon with other materials exhibiting

unique structures and high performance is an important and feasible strategy to achieve excellent performance [31–36]. However, the microfabrication process, especially the microstructuring of pyrolyzed carbon-based composites is challenging and important for realizing the wide applications of pyrolyzed carbon in micro/nano devices.

Among pyrolyzed carbon-based composites, carbon/tin (C/Sn) composite is considered as one of the most promising electrode materials for lithium ion batteries and SCs owing to its high electrical conductivity, chemical stability and relatively high mechanical strength [37–43]. Pyrolyzed carbon with both a high electrical conductivity and a high SSA is difficult to obtain, which are the most important parameters to limit the improvement in SC performance [44]. Sn possesses a higher electrical conductivity ( $\sim 9.09 \times 10^6 \text{ S}\cdot\text{m}^{-1}$  at room temperature) as compared with that of pyrolyzed carbon. Pyrolyzed C/Sn composite exhibits improved electrical conductivity as compared with pyrolyzed carbon, which is promising for solving the issues, such as the slow electrochemical kinetics and sluggish transport rate for obtaining higher efficient transport of electrons. This compositing approach provides a larger specific surface that forms stable electric double layers during charging storage owing to the chemical stability of C/Sn quantum dots (QDs). Ren et al. reported that pyrolyzed C/Sn composite microspheres exhibit a higher mechanical stability as compared with pyrolyzed carbon [45]. In addition, by optimizing the microstructure of C/Sn, its electrochemical performance could be enhanced due to the improved SSA, presence of more active sites, and higher electrical conductivity of the electrode materials [38, 39, 41, 46]. QDs have been utilized to improve the performance of composites owing to their mitigation of volume expansion, controlled solid liquid interface, wetting adhesion, catalysis, adsorption and electron transfer properties [46, 47]. Sn QDs embedded in pyrolyzed carbon allow easy penetration of electrolytes, thereby reducing the internal resistance, which is particularly advantageous for high energy/power density applications [46]. QDs with a higher SSA as compared with other nanostructures are highly promising for compositing with electrodes since the electrons transport pathway can be increased

significantly. Therefore, microstructuring of C/Sn is an effective and important approach for obtaining carbon-based MSCs to realize high performance [48].

In this research, a novel microfabrication process combining controlled chemical synthesis with optimized photolithography and pyrolysis-reduction is investigated for fabricating pyrolyzed porous C/Sn QD microelectrode based MSC (C/Sn-MSC). In this microfabrication process, as-synthesized SnO<sub>2</sub> microspheres were mixed with a photoresist to obtain a uniform photoresist/SnO<sub>2</sub> composite. Then, micropatterning of the composite on Si/SiO<sub>2</sub> substrate was conducted by optimized photolithography, development, and rinse processes. The photoresist was converted to pyrolyzed carbon by pyrolysis performed at a high temperature under inert atmospheric conditions, and SnO<sub>2</sub> was simultaneously reduced to Sn QDs during the pyrolysis process. The as-fabricated MSC exhibits a high specific capacitance (5.79 mF·cm<sup>-2</sup> at a scan rate of 5 mV·s<sup>-1</sup>) and desirable cycling stability (93.3% capacitance retention after 5,000 cyclic voltammetry cycles). The microstructuring of C/Sn QDs achieved by the novel photolithography and pyrolysis-reduction process shows great potential for applications of carbon-based composites, especially for the integration of high-performance micro/nano structures into microdevices, due to its unique advantages for realizing highly stable and multifunctional micropatterned structures.

## 2 Experimental

C/Sn-MSC was fabricated using the microfabrication process described as follows. SnO<sub>2</sub> microspheres were synthesized using a hydrothermal method employing SnCl<sub>4</sub>·5H<sub>2</sub>O as the precursor [49–51]. The photoresist/SnO<sub>2</sub> composite was obtained by mixing SnO<sub>2</sub> microspheres and PR1-9000A photoresist (Futurrex, Inc., Co., Ltd.) through ultrasonic agitation and stirring. Si/SiO<sub>2</sub> substrates with a 300 nm thick SiO<sub>2</sub> layer were cleaned using a typical Radio Corporation of America (RCA) cleaning process. After micropatterning the photoresist/SnO<sub>2</sub> by photolithography, development and rinse, the C/Sn-MSC was fabricated employing pyrolysis-reduction of a micropatterned photoresist/SnO<sub>2</sub> composite at a high temperature (700 and 900 °C) under N<sub>2</sub> atmosphere.

For performing the hydrothermal synthesis of SnO<sub>2</sub> microspheres, SnCl<sub>4</sub>·5H<sub>2</sub>O (3.5 g) was added into deionized (DI) water (70 mL) and stirred for 10 min to obtain a homogeneous solution. NaOH (2.3 g) was then added to the mixture to adjust the pH of the solution to ~12, followed by stirring the solution for 60 min. The solution was then transferred into a Teflon vessel (100 mL) with a stainless steel shell, and the temperature was maintained at 180 °C for 24 h. DI water and ethanol were used to clean the samples several times by centrifugation. After baking the sample at 80 °C for 12 h and grinding with an agate mortar, SnO<sub>2</sub> microspheres were obtained.

The photoresist/SnO<sub>2</sub> (2.0 wt.% SnO<sub>2</sub>) composite was obtained by mixing SnO<sub>2</sub> microspheres with a PR1-9000A photoresist by continuous stirring and ultrasonication carried out for 3 h in order to uniformly disperse the SnO<sub>2</sub> microspheres to the photoresist. The sample was then kept in a vacuum chamber for 1 h to remove air bubbles trapped in the composite. The microfabrication process employed is shown in Fig. 1. Si/SiO<sub>2</sub> substrates were cleaned using a typical RCA cleaning process followed by performing dehydration baking at 145 °C for 30 min. Spin-coating of the photoresist or photoresist/SnO<sub>2</sub> composite was carried out using a spinner via two-step spin-coating to form a uniform film. For obtaining photoresist/SnO<sub>2</sub> film, spin-coating was initially conducted at 1,000 revolution per minute (rpm) for 10 s and then at 4,000 rpm for 40 s, followed by pre-baking the sample at 100 °C for 15 min. Interdigital micropatterns were then obtained by photolithography using a mask aligner. The photoresist/SnO<sub>2</sub> was exposed to a mercury lamp with a dose of 950 mJ·cm<sup>-2</sup>. The

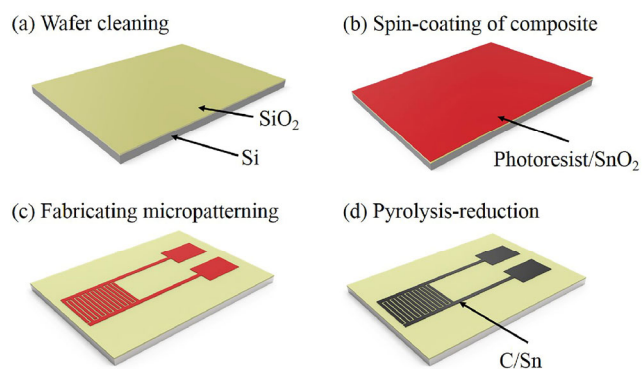


**Figure 1** Microfabrication process of C/Sn-MSC.

development was performed with the RD6 developer (Futurrex, Inc. Co. Ltd.) for 60 s, followed by rinsing 2 times with DI water. After post-baking at 115 °C for 15 min, the samples were pyrolyzed in a tube furnace under N<sub>2</sub> atmosphere. The pyrolysis process was performed in two steps with a continuous N<sub>2</sub> flow in which the samples were initially heated at a rate of 3 °C·min<sup>-1</sup> from room temperature to 300 °C and held at 300 °C for 30 min. The temperature was then raised to the desired value (700 and 900 °C) at a rate of 5 °C·min<sup>-1</sup> followed by keeping the sample at the desired temperature for 60 min. During this pyrolysis process, the photoresist was carbonized to form porous carbon and the SnO<sub>2</sub> microspheres were simultaneously reduced to Sn QDs by pyrolyzed carbon. The samples were eventually cooled down naturally to room temperature in N<sub>2</sub> flow, and the C/Sn-MSC was successfully fabricated. As shown in Figs. 2(a) and 2(b), the fine micropatterns of the photoresist and photoresist/SnO<sub>2</sub> (2 wt.% SnO<sub>2</sub>) are well preserved after pyrolysis.

The electrochemical behaviors of the as-fabricated MSCs were characterized using an Autolab PGSTAT

302N with H<sub>2</sub>SO<sub>4</sub>-PVA as the electrolyte and applying a two-electrode system. The cyclic voltammograms (CV) curves were obtained at scan rates of 5, 10, 50, and 100 mV·s<sup>-1</sup> with a voltage window of 0–0.8 V.

The capacitance of the MSC was calculated by the following equation

$$C = \frac{\int I(V)dV}{2s\Delta V} \quad (1)$$

where  $\int I(V)dV$  is the square of the charge–discharge curves by differentiation,  $s$  is the scan rate, and  $\Delta V$  is the voltage range. The specific areal and volumetric capacitances of MSC can be calculated from Eqs. (2) and (3), respectively

$$C_A = \frac{C}{A} \quad (2)$$

$$C_V = \frac{C}{V} \quad (3)$$

where  $A$  and  $V$  are the area and volume of the microelectrodes, respectively, and the detailed size of the interdigital microelectrodes is shown in Fig. S1 in

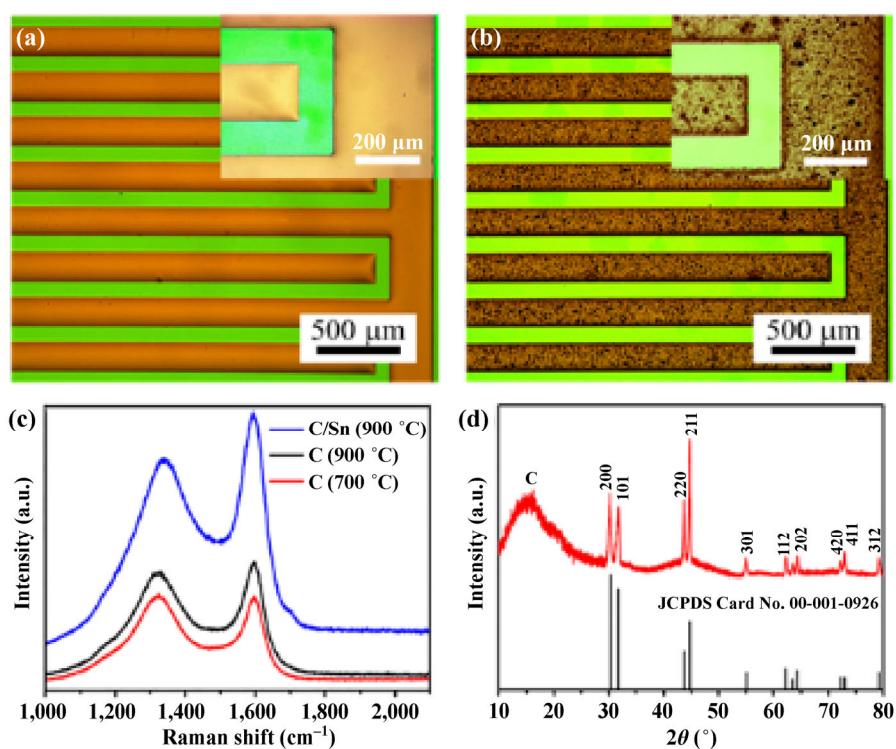


**Figure 2** Optical images of (a) carbon and (b) C/Sn (2 wt.% SnO<sub>2</sub>) obtained after pyrolysis process. (c) Raman spectra of carbon and C/Sn microelectrodes obtained by pyrolysis at different temperatures. (d) XRD pattern of C/Sn obtained by pyrolysis-reduction at 900 °C.

the Electronic Supplementary Material (ESM). The capacitance of MSC is calculated by employing CV measurements at scan rates of 5–100 mV·s<sup>-1</sup>.

X-ray diffraction (XRD) patterns of the as-synthesized samples were recorded using an X-ray diffractometer (Bruker D8 Discover), and the morphologies of the samples were characterized using scanning electron microscopy (SEM, JEOL JSM-7100F). Transmission electron microscopy (TEM) and high-resolution TEM (HRTEM) images were recorded with a JEM-2100F microscope. Raman spectra were obtained using a Renishaw Raman microscope (Renishaw RM-1000).

### 3 Results and discussion

Figure S2 (in the ESM) shows the typical field-emission SEM (FESEM) images of the synthesized SnO<sub>2</sub> microspheres. The SnO<sub>2</sub> microspheres exhibit a uniform diameter of ~1.5 μm. XRD characterization is employed for the phase analysis of the SnO<sub>2</sub> microspheres (Fig. S3 in the ESM). The diffraction peaks matched well with the standard values (JCPDS Card No. 01-088-0287) ( $a = b = 0.4737$  nm,  $c = 0.3186$  nm), demonstrating the high crystallinity of the tetragonal SnO<sub>2</sub> microspheres.

Figures 2(a) and 2(b) show the optical microscope images of carbon and C/Sn QD (2 wt.% SnO<sub>2</sub>) microelectrodes obtained by pyrolysis at 900 °C, respectively. The structures of the fabricated interdigital microelectrodes are well preserved, and fine micropatterns with no cracks are obtained, indicating that the microfabrication process is highly suitable for the microstructuring of this kind of carbon-based composites. Raman spectra of the photoresist-derived carbon and C/Sn microelectrodes obtained by pyrolysis at different temperatures are shown in Fig. 2(c). Disorder-induced band (D-band) and graphitic band (G-band) are observed. The D-band observed at ~1,300 cm<sup>-1</sup> indicates the graphite microcrystallinity due to enhanced double resonance. The peak at ~1,600 cm<sup>-1</sup> corresponds to G-band, which is ascribed to the bond stretching of sp<sup>2</sup> carbon atoms present in the olefinic chains or the aromatic rings [10]. The ratio of  $I_G$  to  $I_D$  indicates the degree of graphitization of carbon. For the photoresist-derived carbon obtained by pyrolysis at 700 °C, an  $(I_G/I_D)_{700}$  value of 0.93 is

achieved, while at 900 °C, an  $(I_G/I_D)_{900}$  value of 1.10 is obtained, indicating that the graphitization degree increases as the pyrolysis temperature increases. Furthermore, for the sample pyrolyzed at 900 °C,  $(I_G/I_D)_{C/Sn} = 1.20 > (I_G/I_D)_{carbon} = 1.10$ . Thus, the graphitization of C/Sn is higher than that of pyrolyzed carbon. The HRTEM image of the C/Sn microelectrodes reveals a lattice spacing of ~3.3 Å corresponding to the (002) crystal plane of graphite near the interface of Sn QDs (Fig. S4 in the ESM). Thus, the graphitization degree of pyrolyzed carbon could be enhanced by compositing with Sn, which is attributed to the catalytic effect of Sn QDs.

As shown in Fig. 2(d), the XRD pattern of C/Sn exhibits a broad maxima (wide peak) at around 15°, demonstrating the existence of amorphous phase in the sample. According to a previous study, the amorphous phase should correspond to amorphous carbon [52]. As shown in the XRD pattern, the existence of Sn is confirmed since the obtained sharp peaks match well with those of tetragonal Sn (JCPDS Card No. 00-001-0926), which is formed in the pyrolysis-reduction process.

Energy-dispersive X-ray spectrometry (EDS) mapping analysis results of the microelectrodes are shown in Figs. 3(a)–3(d), confirming the homogeneous distribution of Sn in the C/Sn microelectrodes. The inexistence of O in C/Sn microelectrodes demonstrates the complete reduction of SnO<sub>2</sub> to Sn. The SEM image of the C/Sn microelectrodes obtained using photoresist/SnO<sub>2</sub> (2 wt.% SnO<sub>2</sub>) as the starting material is shown in Fig. 3(e). After pyrolysis, the shape and dimension of the fine micropatterns are unchanged without forming any cracks, indicating that the microfabrication process can be used for obtaining fine microelectrodes with a high stability and uniformity.

In addition, the microelectrodes are well preserved on the Si/SiO<sub>2</sub> substrate because of the high adhesion between the microelectrode and substrate, which is in agreement with previous studies [10, 11]. As shown in Fig. 3(e), Sn nanoparticles (diameter of ~15 nm) are observed on the surface of the C/Sn microelectrode. A TEM image of the C/Sn QD microelectrode is shown in Fig. 3(f), in which Sn QDs with diameter of ~3 nm are uniformly dispersed in pyrolyzed carbon. Furthermore, the HRTEM image (Fig. 3(g)) demonstrates an

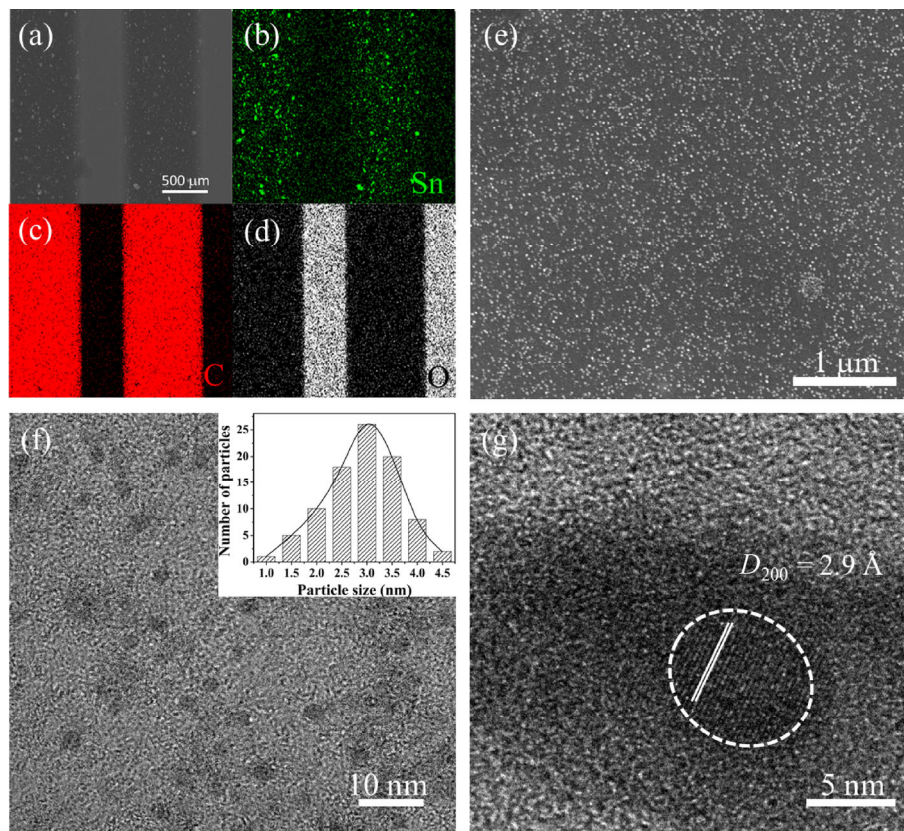


**Figure 3** (a)–(d) EDS elemental mapping of Sn, C, and O. (e) SEM image of the C/Sn QD microelectrode. (f)–(g) TEM and HRTEM images of C/Sn QDs.

interplanar spacing of  $\sim 2.9 \text{ \AA}$  corresponding to (200) crystal planes of Sn that can be indexed to the XRD peak of  $30.7^\circ$  (JCPDS Card No. 00-001-0926).

To investigate the mechanism of Sn QDs (Fig. 4(a)) and Sn nanoparticles formation further, thermogravimetric (TG) analysis and differential scanning calorimetry (DSC) measurements were conducted (Fig. 4(b)). As shown in Fig. 4(a), pyrolyzed carbon is obtained by carbonization and  $\text{SnO}_2$  is reduced to Sn with an increase in temperature in the pyrolysis-reduction process under  $\text{N}_2$  atmosphere [46]. Sn

transforms to gaseous Sn in the pores of the carbon matrix, so there is no obvious DSC peak in the inset of Fig. 4(b), resulting from comparatively distinct carbonization.

Sn transforms to gaseous Sn due to the volatile process occurring at high temperature, which has been reported in a previous study [53]. Sn QDs are obtained from gaseous Sn with a decrease in temperature, which is associated with the exothermic DSC peak at  $\sim 800.08^\circ \text{C}$  (Fig. 4(b)). In addition, Sn nanoparticles are formed at the surface of electrode

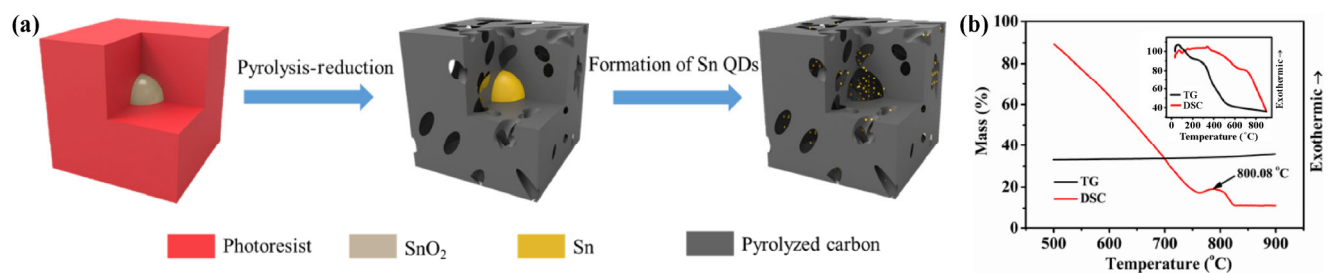


**Figure 4** (a) Schematic of the Sn QD formation process. (b) TG-DSC curves of photoresist/ $\text{SnO}_2$  (2 wt.%  $\text{SnO}_2$ ) recorded with a decrease in temperature. Inset shows data for an increase in temperature.

as respectively more gaseous Sn is present over the surface of microelectrode. After this process, pores with a diameter of  $\sim 1.5 \mu\text{m}$  are formed in pyrolyzed carbon, which matches well with the size of  $\text{SnO}_2$  microspheres (Fig. S5 in the ESM), and smaller pores connecting the bigger pores are also formed.

The electrochemical performance of C/Sn-MSC was investigated using a 1 M PVA/ $\text{H}_2\text{SO}_4$  gel electrolyte employing CV and electrochemical impedance spectroscopy (EIS). As shown in Fig. 5, the specific capacitance of C/Sn-MSC is higher as compared with that of the pyrolyzed carbon-based MSC (C-MSC) fabricated by a similar process. The interfaces between carbon and Sn QDs contribute towards improving the SSA and electrical conductivity of microelectrodes as compared with carbon microelectrodes.

CV curves of the C-MSC and C/Sn-MSC recorded at scan rates of 5 and  $100 \text{ mV}\cdot\text{s}^{-1}$  are shown in Figs. 5(a) and 5(b), respectively. CV curves with a typical rectangular shape are obtained, suggesting the electrochemical double layer capacitor (EDLC) mechanism of C-MSC and C/Sn-MSC. As described above, the current density of C/Sn-MSC is much higher than that of C-MSC at different scan rates. C/Sn-MSC exhibits an areal specific capacitance of  $5.79 \text{ mF}\cdot\text{cm}^{-2}$

at a scan rate of  $5 \text{ mV}\cdot\text{s}^{-1}$  as calculated from the CV curve (the volumetric specific capacitance of  $22.44 \text{ F}\cdot\text{cm}^{-3}$ ), which is about 2.5 times higher than that of C-MSC ( $1.67 \text{ mF}\cdot\text{cm}^{-2}$ ). This is higher than the corresponding values reported earlier for nanocarbon-based MSCs (as shown in Table S1 in the ESM).

Figure 5(c) illustrates the dependence of areal capacitance on the scan rate in C-MSC and C/Sn-MSC. On increasing the scan rate from 5 to  $100 \text{ mV}\cdot\text{s}^{-1}$ , C/Sn-MSC exhibits  $\sim 4$  times higher areal capacitance than that of C-MSC, indicating the relatively higher rate capability of C/Sn-MSC.

To understand the reason for the enhanced electrochemical performance of C/Sn-MSC, EIS measurements of C-MSC and C/Sn-MSC were performed in the frequency range of 0.01–0.1 MHz. The Nyquist plot shown in Fig. 5(d) reveals that at high frequencies, the additional large semicircle for the C-MSC is observed, which is much larger than that of C/Sn-MSC. We attribute the high resistance to the poor electrical conductivity of pyrolyzed carbon and the higher electrical conductivity of C/Sn compared with that of carbon.

Figure 6(a) shows the CV curves of C/Sn-MSC recorded at different scan rates (from 5 to  $100 \text{ mV}\cdot\text{s}^{-1}$ ),

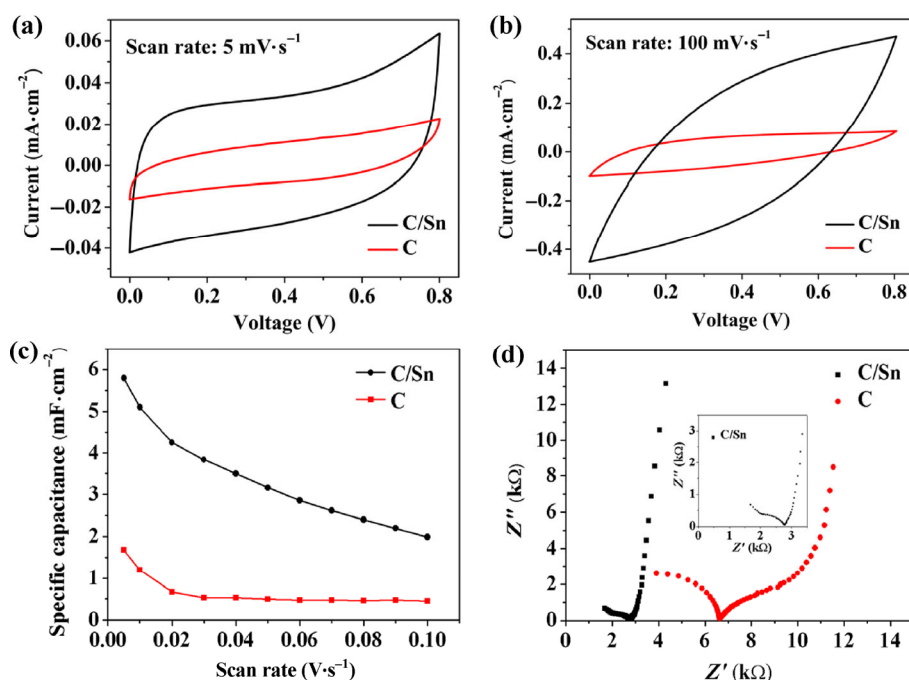


**Figure 5** (a) and (b) CV curves of C-MSC and C/Sn-MSC at different scan rates. (c) Specific capacitance of C-MSC and C/Sn-MSC calculated from the CV curves obtained at different scan rates. (d) AC impedance spectra of C-MSC and C/Sn-MSC.

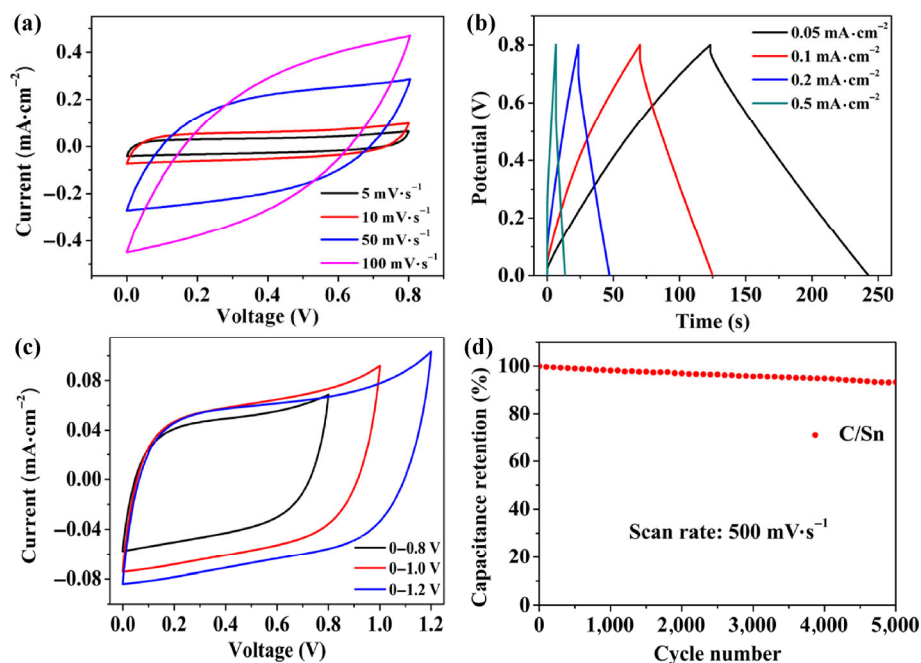


**Figure 6** (a) CV curves of C/Sn-MSC at different scan rates. (b) Charge–discharge curves of C/Sn-MSC at different current densities. (c) CV curves of C/Sn-MSC at a scan rate of  $5 \text{ mV}\cdot\text{s}^{-1}$  with different voltage windows. (d) Cycling performance of C/Sn-MSC.

indicating a good electrochemical stability and rapid response on voltage reversal. The nearly symmetrical charge–discharge curves of C/Sn-MSC (Fig. 6(b)) obtained at a gradient current density (from  $0.05$  to  $0.5 \text{ mA}\cdot\text{cm}^{-2}$ ) indicate the high reversibility of the as-fabricated MSC. CV curves recorded at different voltage windows are shown in Fig. 6(c). The typical rectangular shapes of the curves are maintained with an increase in the voltage range, demonstrating that C/Sn-MSC exhibits excellent electrochemical stability even at a high voltage ( $1.2 \text{ V}$ ). The areal capacitance of C/Sn-MSC calculated from the CV curve at the voltage window of  $0\text{--}1.2 \text{ V}$  increases to  $7.65 \text{ mF}\cdot\text{cm}^{-2}$  at a scan rate of  $5 \text{ mV}\cdot\text{s}^{-1}$ . In addition, the cycling performance of C/Sn-MSC shown in Fig. 6(d) indicates a small capacitance loss occurring during the cycling process and a remarkable long-term cyclability of  $93.3\%$  capacitance retention achieved after  $5,000$  CV cycles at a scan rate of  $0.5 \text{ V}\cdot\text{s}^{-1}$ , demonstrating the excellent cycling performance of C/Sn-MSC.

## 4 Conclusions

A C/Sn QD microelectrode-based MSC is designed and fabricated using a novel microfabrication process

involving photolithography and pyrolysis-reduction. In this pyrolysis-reduction process, some of the carbon atoms is consumed by  $\text{SnO}_2$ , and  $\text{SnO}_2$  microspheres are reduced to form Sn QDs (diameter:  $\sim 3 \text{ nm}$ ) simultaneously. The C/Sn QDs serve both as a current collector and electrochemically active electrode in the MSC. The electrochemical performance of the C/Sn-MSC is significantly improved as compared with that of C-MSC. The enhanced performance of the C/Sn-MSC is attributed to the high electrical conductivity of Sn QDs uniformly dispersed in the microelectrodes and improved SSA of microelectrodes. The microstructuring of C/Sn QDs using the novel photolithography and pyrolysis-reduction process is investigated and developed, which exhibits great potential in the further development of high-performance MSCs or other microdevices/systems based on carbon-based composites.

## Acknowledgements

This work was supported by the National Key Research and Development Program of China (Nos. 2016YFA0202603 and 2016YFA0202604), the National Basic Research Program of China (No. 2013CB934103),

the Programme of Introducing Talents of Discipline to Universities (No. B17034), the National Natural Science Foundation of China (Nos. 51502227, 51579198 and 51521001), the National Natural Science Fund for Distinguished Young Scholars (No. 51425204), the China Postdoctoral Science Foundation (No. 2015T80845), the Hubei Province Natural Science Fund (No. 2016CFB582), the Fundamental Research Funds for the Central Universities (WUT: 2016III001 and 2016III005). Prof. Liang He and Prof. Liqiang Mai gratefully acknowledged financial support from China Scholarship Council (Nos. 201606955094 and 201606955096).

**Electronic Supplementary Material:** Supplementary material (the detailed size of the interdigital micro-electrodes; SEM images and XRD pattern of SnO<sub>2</sub> microspheres; HRTEM image and SEM cross section image of C/Sn QDs microelectrode) is available in the online version of this article at <https://doi.org/10.1007/s12274-017-1587-2>.

## References

- [1] Cai, Z. Y.; Xu, L.; Yan, M. Y.; Han, C. H.; He, L.; Hercule, K. M.; Niu, C. J.; Yuan, Z. F.; Xu, W. W.; Qu, L. B. et al. Manganese oxide/carbon yolk-shell nanorod anodes for high capacity lithium batteries. *Nano Lett.* **2015**, *15*, 738–744.
- [2] Béguin, F.; Presser, V.; Balducci, A.; Frackowiak, E. Carbons and electrolytes for advanced supercapacitors. *Adv. Mater.* **2014**, *26*, 2219–2251.
- [3] Hsia, B.; Kim, M. S.; Vincent, M.; Carraro, C.; Maboudian, R. Photoresist-derived porous carbon for on-chip micro-supercapacitors. *Carbon* **2013**, *57*, 395–400.
- [4] Ren, S. Z.; Wang, M.; Xu, M. L.; Yang, Y.; Jia, C. Y.; Hao, C. Fabrication of high-performance supercapacitors based on hollow SnO<sub>2</sub> microspheres. *J. Solid State Electrochem.* **2014**, *18*, 909–916.
- [5] Jang, J.; Bae, J.; Choi, M.; Yoon, S.-H. Fabrication and characterization of polyaniline coated carbon nanofiber for supercapacitor. *Carbon* **2005**, *43*, 2730–2736.
- [6] Huang, P.; Lethien, C.; Pinaud, S.; Brousse, K.; Laloo, R.; Turq, V.; Respaud, M.; Demortière, A.; Daffos, B.; Taberna, P. L. et al. On-chip and freestanding elastic carbon films for micro-supercapacitors. *Science* **2016**, *351*, 691–695.
- [7] Niu, Z. Q.; Zhou, W. Y.; Chen, X. D.; Chen, J.; Xie, S. S. Highly compressible and all-solid-state supercapacitors based on nanostructured composite sponge. *Adv. Mater.* **2015**, *27*, 6002–6008.
- [8] Liu, L. L.; Niu, Z. Q.; Chen, J. Design and integration of flexible planar micro-supercapacitors. *Nano Res.* **2017**, *10*, 1524–1544.
- [9] Liu, L. L.; Niu, Z. Q.; Chen, J. Unconventional supercapacitors from nanocarbon-based electrode materials to device configurations. *Chem. Soc. Rev.* **2016**, *45*, 4340–4363.
- [10] Yin, C.; He, L.; Wang, Y. F.; Liu, Z. H.; Zhang, G. B.; Zhao, K. N.; Tang, C. J.; Yan, M. Y.; Han, Y. L.; Mai, L. Q. Pyrolyzed carbon with embedded NiO/Ni nanospheres for applications in microelectrodes. *RSC Adv.* **2016**, *6*, 43436–43441.
- [11] Yang, Y. J.; He, L.; Tang, C. J.; Hu, P.; Hong, X. F.; Yan, M. Y.; Dong, Y. X.; Tian, X. C.; Wei, Q. L.; Mai, L. Q. Improved conductivity and capacitance of interdigital carbon microelectrodes through integration with carbon nanotubes for micro-supercapacitors. *Nano Res.* **2016**, *9*, 2510–2519.
- [12] He, L.; Toda, M.; Kawai, Y.; Miyashita, H.; Omori, M.; Hashida, T.; Berger, R.; Ono, T. Fabrication of CNT-carbon composite microstructures using Si micromolding and pyrolysis. *Microsyst. Technol.* **2014**, *20*, 201–208.
- [13] De Volder, M. F. L.; Vanswevelt, R.; Wagner, P.; Reynaerts, D.; van Hoof, C.; Hart, A. J. Hierarchical carbon nanowire microarchitectures made by plasma-assisted pyrolysis of photoresist. *ACS Nano* **2011**, *5*, 6593–6600.
- [14] Wei, L.; Nitta, N.; Yushin, G. Lithographically patterned thin activated carbon films as a new technology platform for on-chip devices. *ACS Nano* **2013**, *7*, 6498–6506.
- [15] Jariwala, D.; Sangwan, V. K.; Lauhon, L. J.; Marks, T. J.; Hersam, M. C. Carbon nanomaterials for electronics, optoelectronics, photovoltaics, and sensing. *Chem. Soc. Rev.* **2013**, *42*, 2824–2860.
- [16] Sevilla, M.; Mokaya, R. Energy storage applications of activated carbons: Supercapacitors and hydrogen storage. *Energy Environ. Sci.* **2014**, *7*, 1250–1280.
- [17] Niu, Z. Q.; Zhang, L.; Liu, L. L.; Zhu, B. W.; Dong, H. B.; Chen, X. D. All-solid-state flexible ultrathin micro-supercapacitors based on graphene. *Adv. Mater.* **2013**, *25*, 4035–4042.
- [18] Beidaghi, M.; Wang, C. L. Micro-supercapacitors based on three dimensional interdigital polypyrrole/C-MEMS electrodes. *Electrochim. Acta* **2011**, *56*, 9508–9514.
- [19] Wei, L.; Sevilla, M.; Fuertes, A. B.; Mokaya, R.; Yushin, G. Polypyrrole-derived activated carbons for high-performance electrical double-layer capacitors with ionic liquid electrolyte. *Adv. Funct. Mater.* **2012**, *22*, 827–834.
- [20] Malladi, K.; Wang, C. L.; Madou, M. Fabrication of suspended carbon microstructures by e-beam writer and pyrolysis. *Carbon* **2006**, *44*, 2602–2607.
- [21] Galobardes, F.; Wang, C.; Madou, M. Investigation on the

- solid electrolyte interface formed on pyrolyzed photoresist carbon anodes for C-MEMS lithium-ion batteries. *Diam. Relat. Mater.* **2006**, *15*, 1930–1934.
- [22] Lu, X. X.; Yang, F.; Geng, X.; Xiao, P. Enhanced cyclability of amorphous carbon-coated SnO<sub>2</sub>-graphene composite as anode for Li-ion batteries. *Electrochim. Acta* **2014**, *147*, 596–602.
- [23] Lee, J. A.; Lee, S. W.; Lee, K.-C.; Park, S. I.; Lee, S. S. Fabrication and characterization of freestanding 3D carbon microstructures using multi-exposures and resist pyrolysis. *J. Micromech. Microeng.* **2008**, *18*, 035012.
- [24] Beidaghi, M.; Chen, W.; Wang, C. L. Electrochemically activated carbon micro-electrode arrays for electrochemical micro-capacitors. *J. Power Sources* **2011**, *196*, 2403–2409.
- [25] Min, H.-S.; Park, B. Y.; Taherabadi, L.; Wang, C. L.; Yeh, Y.; Zaouk, R.; Madou, M. J.; Dunn, B. Fabrication and properties of a carbon/polypyrrole three-dimensional microbattery. *J. Power Sources* **2008**, *178*, 795–800.
- [26] Wei, L.; Yushin, G. Nanostructured activated carbons from natural precursors for electrical double layer capacitors. *Nano Energy* **2012**, *1*, 552–565.
- [27] Chen, W.; Beidaghi, M.; Penmatsa, V.; Bechtold, K.; Kumari, L.; Li, W. Z.; Wang, C. L. Integration of carbon nanotubes to C-MEMS for on-chip supercapacitors. *IEEE Trans. Nanotechnol.* **2010**, *9*, 734–740.
- [28] Wang, C. L.; Jia, G. Y.; Taherabadi, L. H.; Madou, M. J. A novel method for the fabrication of high-aspect ratio C-MEMS structures. *J. Microelectromech. Syst.* **2005**, *14*, 348–358.
- [29] Schueller, O. J. A.; Brittain, S. T.; Whitesides, G. M. Fabrication of glassy carbon microstructures by soft lithography. *Sensor Actuat. A-Phys.* **1999**, *72*, 125–139.
- [30] Jiang, H.; Lee, P. S.; Li, C. Z. 3D carbon based nanostructures for advanced supercapacitors. *Energy Environ. Sci.* **2013**, *6*, 41–53.
- [31] McCreery, R. L. Advanced carbon electrode materials for molecular electrochemistry. *Chem. Rev.* **2008**, *108*, 2646–2687.
- [32] Li, J.; Le, D. B.; Ferguson, P. P.; Dahn, J. R. Lithium polyacrylate as a binder for tin–cobalt–carbon negative electrodes in lithium-ion batteries. *Electrochim. Acta* **2010**, *55*, 2991–2995.
- [33] Tang, J.; Liu, J.; Torad, N. L.; Kimura, T.; Yamauchi, Y. Tailored design of functional nanoporous carbon materials toward fuel cell applications. *Nano Today* **2014**, *9*, 305–323.
- [34] Lee, J. A.; Lee, K. C.; Park, S. I.; Lee, S. S. The fabrication of carbon nanostructures using electron beam resist pyrolysis and nanomachining processes for biosensing applications. *Nanotechnology* **2008**, *19*, 215302.
- [35] Sheeja, D.; Tay, B. K.; Lau, S. P.; Yu, L. J.; Miao, J. M.; Chua, H. C.; Milne, W. I. Fabrication of smooth amorphous carbon micro-cantilevers by lift-off. *Sensor Actuat. B-Chem.* **2004**, *98*, 275–281.
- [36] Yan, S.; Wu, Q. S. Micropored Sn-SnO<sub>2</sub>/carbon heterostructure nanofibers and their highly sensitive and selective C<sub>2</sub>H<sub>5</sub>OH gas sensing performance. *Sensor Actuat. B-Chem.* **2014**, *205*, 329–337.
- [37] Luo, B.; Wang, B.; Liang, M. H.; Ning, J.; Li, X. L.; Zhi, L. J. Reduced graphene oxide-mediated growth of uniform tin-core/carbon-sheath coaxial nanocables with enhanced lithium ion storage properties. *Adv. Mater.* **2012**, *24*, 1405–1409.
- [38] Sun, L. M.; Wang, X. H.; Susantyoko, R. A.; Zhang, Q. High performance binder-free Sn coated carbon nanotube array anode. *Carbon* **2015**, *82*, 282–287.
- [39] Noh, M.; Kwon, Y.; Lee, H.; Cho, J.; Kim, Y.; Kim, M. G. Amorphous carbon-coated tin anode material for lithium secondary battery. *Chem. Mater.* **2005**, *17*, 1926–1929.
- [40] Chen, S. Q.; Chen, P.; Wu, M. H.; Pan, D. Y.; Wang, Y. Graphene supported Sn–Sb@carbon core-shell particles as a superior anode for lithium ion batteries. *Electrochem. Commun.* **2010**, *12*, 1302–1306.
- [41] Liu, C.-J.; Huang, H.; Cao, G.-Z.; Xue, F.-H.; Paredes Camacho, R. A.; Dong, X.-L. Enhanced electrochemical stability of Sn-carbon nanotube nanocapsules as lithium-ion battery anode. *Electrochim. Acta* **2014**, *144*, 376–382.
- [42] Guo, B. K.; Shu, J.; Tang, K.; Bai, Y.; Wang, Z. X.; Chen, L. Q. Nano-Sn/hard carbon composite anode material with high-initial coulombic efficiency. *J. Power Sources* **2008**, *177*, 205–210.
- [43] Lee, K. T.; Jung, Y. S.; Oh, S. M. Synthesis of tin-encapsulated spherical hollow carbon for anode material in lithium secondary batteries. *J. Am. Chem. Soc.* **2003**, *125*, 5652–5653.
- [44] Simon, P.; Gogotsi, Y. Materials for electrochemical capacitors. *Nat. Mater.* **2008**, *7*, 845–854.
- [45] Yang, Y.; Ren, S. Z.; Ma, S. B.; Hao, C.; Ji, M. The synthesis of ordered Sn-C composite microspheres and their mechanical properties. *Colloid. Surf. A* **2015**, *471*, 81–85.
- [46] Zhang, G. H.; Zhu, J.; Zeng, W.; Hou, S. C.; Gong, F. L.; Li, F.; Li, C. C.; Duan, H. G. Tin quantum dots embedded in nitrogen-doped carbon nanofibers as excellent anode for lithium-ion batteries. *Nano Energy* **2014**, *9*, 61–70.
- [47] Ramana, B. V.; Das, A.; Dhara, S.; Amirthapandian, S.; Tyagi, A. K. Synthesis and surface functionalization of SnO<sub>2</sub> nanoparticles and their superhydrophobic coatings. *Sci. Adv. Mater.* **2013**, *5*, 865–872.
- [48] Egashira, M.; Takatsuji, H.; Okada, S.; Yamaki, J.-I.

- Properties of containing Sn nanoparticles activated carbon fiber for a negative electrode in lithium batteries. *J. Power sources* **2002**, *107*, 56–60.
- [49] Zhao, K. N.; Zhang, L.; Xia, R.; Dong, Y. F.; Xu, W. W.; Niu, C. J.; He, L.; Yan, M. Y.; Qu, L. B.; Mai, L. Q. SnO<sub>2</sub> quantum dots@graphene oxide as a high-rate and long-life anode material for lithium-ion batteries. *Small* **2016**, *12*, 588–594.
- [50] Zhang, L.; Zhao, K. N.; Xu, W. W.; Dong, Y. F.; Xia, R.; Liu, F. N.; He, L.; Wei, Q. L.; Yan, M. Y.; Mai, L. Q. Integrated SnO<sub>2</sub> nanorod array with polypyrrole coverage for high-rate and long-life lithium batteries. *Phys. Chem. Chem. Phys.* **2015**, *17*, 7619–7623.
- [51] Xu, W. W.; Zhao, K. N.; Niu, C. J.; Zhang, L.; Cai, Z. Y.; Han, C. H.; He, L.; Shen, T.; Yan, M. Y.; Qu, L. B. et al. Heterogeneous branched core-shell SnO<sub>2</sub>-PANI nanorod arrays with mechanical integrity and three dimensional electron transport for lithium batteries. *Nano Energy* **2014**, *8*, 196–204.
- [52] Zhou, P.; Yang, X.; He, L.; Hao, Z. M.; Luo, W.; Xiong, B.; Xu, X.; Niu, C. J.; Yan, M. Y.; Mai, L. Q. The young's modulus of high-aspect-ratio carbon/carbon nanotube composite microcantilevers by experimental and modeling validation. *Appl. Phys. Lett.* **2015**, *106*, 111908.
- [53] Chen, M. M.; Xia, X. X.; Wang, Z. L.; Li, Y. L.; Li, J. J.; Gu, C. Z. Rectifying behavior of individual SnO<sub>2</sub> nanowire by different metal electrode contacts. *Microelectron. Eng.* **2008**, *85*, 1379–1381.